

Data-Driven Modeling of Ground Effect For UAV Landing on a Vertical Oscillating Platform

Binglin He, Heng Zhang, Song Liu *Member, IEEE*, and Yang Wang *Member, IEEE*

Abstract—Due to the complex aerodynamic effects resulting from the interaction between multi-rotor airflow and the landing platform, i.e. the ground effect, achieving rapid and precise landings of multi-rotor unmanned aerial vehicles (UAVs) on moving platforms becomes highly challenging. In this paper, we propose a data-driven method for modeling Ground Effect Forces (GEF) during UAV landings on a vertically oscillating platform. Then, based on the established GEF model, we introduce a flight control algorithm incorporating feedforward compensation for ground effect to facilitate faster and smoother UAV landings. Our proposed method offers two significant innovations when compared to existing approaches. Firstly, we consider the vertical oscillation of the platform, which makes the GEF acting on UAVs more complex in such environments. Secondly, our proposed model is sparse, interpretable, and has low computation cost, rendering it control-friendly for UAV applications. Experimental results validate the accuracy of the model. Additionally, successful rapid and stable landings achieved by UAVs on both ground and vertically oscillating platforms further demonstrate the effectiveness of the algorithm.

I. INTRODUCTION

In contemporary times, Unmanned Aerial Vehicles (UAVs) play a crucial role in various scenarios [1]–[3]. Particularly, in maritime missions, UAVs have proven to be highly valuable when employed in various specialized tasks such as search and rescue operations [4], survey missions [5], and environmental monitoring [6]. One critical aspect among these is ensuring the safe landing of UAVs on a vertically oscillating platform. Aside from the UAV’s nonlinear characteristics and limited platform size, the intricate interactions between rotor airflow during landing and the oscillating platform may result in flight instability or even catastrophic failure [7, chapt.4]. This phenomenon, known as the Ground Effect (GE), poses a great challenge that must be addressed to achieve rapid and smooth autonomous landings on vertical oscillating platforms.

There are various approaches to the autonomous control of unmanned aerial vehicles (UAVs), including fault-tolerant control strategies [8], model predictive methods [9], active disturbance rejection techniques [10], among others [11],

*This work was in part supported by the National Natural Science Foundation of China under Grant 62303321. (Corresponding author: Song Liu and Yang Wang.)

B. He and H. Zhang are with the School of Information Science and Technology, ShanghaiTech University, Shanghai 201210, China (email: hebl2022, zhangheng1@shanghaitech.edu.cn)

S. Liu and Y. Wang are with the School of Information Science and Technology, ShanghaiTech University, Shanghai 201210, China, and with Shanghai Engineering Research Center of Intelligent Vision and Imaging, Shanghai, China (e-mail: liusong, wangyang4@shanghaitech.edu.cn)

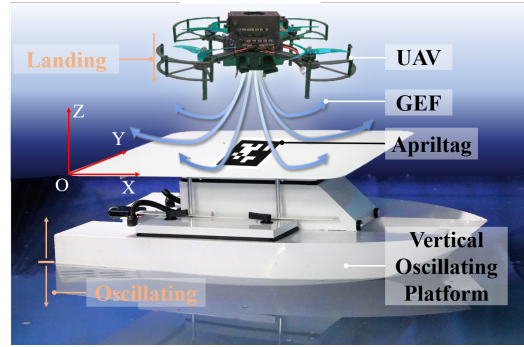


Fig. 1: GEF, considered as f_a , occurs during the landing process of UAV landing on the vertical oscillating platform.

[12]. These methods can all be applied to UAV landing scenarios. However, under such control strategies, due to feedback delays and the influence of GE, the UAV typically necessitates a gradual descent to ensure a smooth and safe landing. Consequently, the modeling of GEF and the incorporation of feedforward compensation have emerged as more effective approaches. However, modeling the GE during UAV landing presents significant challenges due to the intricate aerodynamic interactions. The prevailing approach in existing solutions relies heavily on empirical formulas [13], [14]. Despite their effectiveness, the acquisition of an accurate model still necessitates a substantial amount of real-world data for identifying unknown parameters. In response to this challenge, alternative solutions based on neural networks (NN) [15] aim to directly derive data-driven models. However, the existing empirical GEF models exhibit some limitations in terms of accuracy (see Fig. 2), while black-box modeling approaches can not ensure stability. Furthermore, it is worth noting that the majority of current GEF models are developed based on the landing of unmanned aerial vehicles on fixed platforms, with very few precise models developed for landing on vertical oscillation platforms.

Motivated by the above discussion, this study investigates the modeling problem of ground effect forces during the landing process of UAVs on a vertical vibrating platform. A data-driven modeling approach and a landing scheme based on feedforward control are proposed. Compared with existing methods [14], [15], our approach features two distinctive innovations. Firstly, we account for platforms with vertical vibrations, on which UAVs experience more complex GEF. Moreover, our proposed model is sparse and interpretable, allowing for stability analysis in conjunction with various control methods, meanwhile, its sparsity ensures successful implementation on low computational power UAV platforms.

Notation: In this article, \mathbb{R} denotes the set of real numbers, \mathbb{R}^n and $\mathbb{R}^{m \times n}$ denote the set of n -dimensional vectors and $m \times n$ matrices, respectively. The function $S(\cdot)$ represents the skew-symmetric mapping. Given $x \in \mathbb{R}^n$, $\|x\| := (x_1^2 + \dots + x_n^2)^{1/2}$ is the Euclidean norm. $\mathbf{0} \in \mathbb{R}^n$ is the vector whose all elements are zeros. s is the Laplace operator. g denotes the acceleration of gravity.

II. PROBLEM STATEMENT

In this work, our primary emphasis lies in modeling the Ground Effect Force (GEF) concerning the vertical landing problem of Unmanned Aerial Vehicles (UAVs). To develop, implement, and validate the proposed modeling scheme, we employ a quadrotor. This section will commence by providing a concise overview of the system dynamics, followed by an explanation of the control objective.

A. UAV Model

Consider a model of UAV translation described as [16]:

$$\begin{aligned}\dot{\mathbf{p}} &= \mathbf{v} \\ m\dot{\mathbf{v}} &= mg + \mathbf{f}_u + \mathbf{f}_a\end{aligned}\quad (1)$$

where $\mathbf{p} := [x_q, y_q, z_q]^\top \in \mathbb{R}^3$ represents the global coordinates of UAV and $\mathbf{v} := [v_{x,q}, v_{y,q}, v_{z,q}]^\top \in \mathbb{R}^3$ represents the velocity. m is the mass of UAV. $\mathbf{g} := [0, 0, g]^\top \in \mathbb{R}^3$ corresponds to the gravity vector. $\mathbf{f}_u := [f_x, f_y, f_z]^\top \in \mathbb{R}^3$. $\mathbf{f}_a := [f_{a,x}, f_{a,y}, f_{a,z}]^\top \in \mathbb{R}^3$ denotes the residual aerodynamic force. In particular, it is the Z -axis component of the aerodynamic force \mathbf{f}_a that is the primary focus of consideration in this study. This force pertains to the GEF generated during the vertical oscillations of UAV landings, hereafter referred to as GEF and denoted as $f_{GEF} \in \mathbb{R}$ in this paper. It is important to note that this force can have a significant impact on the flight performance, as depicted in Fig. 1.

B. Ground Effect (GE)

Understanding and effective utilization of GE is crucial for enhancing the landing performance [15]. However, due to the nonlinear dynamics of UAVs, system uncertainties, and complex aerodynamic interaction, modeling the ground effect during the UAV landing process becomes exceedingly challenging. The majority of existing solutions rely on empirical formulas [17] such as

$$\hat{f}_{GEF}^e = \frac{\mu \left(\frac{D}{8z} \right)^2}{1 - \mu \left(\frac{D}{8z} \right)^2} T \quad (2)$$

where $T \in \mathbb{R}$ denotes the thrust generated by propellers in the absence of GE, $\hat{f}_{GEF}^e \in \mathbb{R}$ is the estimated GEF. $z \in \mathbb{R}$ is the relative height between UAV and the platform. D is the rotor's diameter. μ is a constant coefficient depending on the number and arrangement of propellers.

C. Objective

Despite its effectiveness, the existing empirical models are predominantly derived from stationary ground conditions.

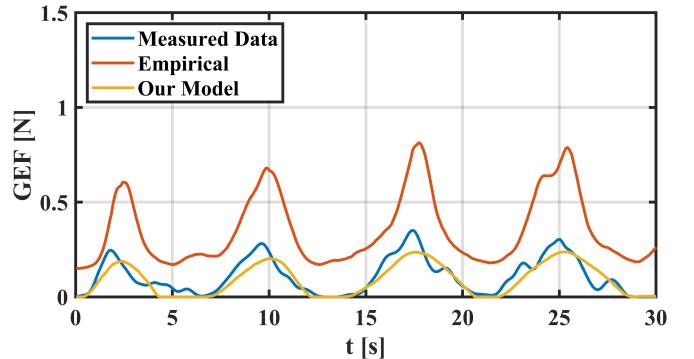


Fig. 2: Blue, orange and yellow lines represent the measured f_{GEF} , \hat{f}_{GEF}^e and \hat{f}_{GEF} respectively. We can see \hat{f}_{GEF}^e estimated by the empirical formula [17] is inaccurate while the platform is undergoing oscillating at a speed of 0.08 m/s and T is set to 12 N. Meanwhile, our GEF model achieves accurate estimation.

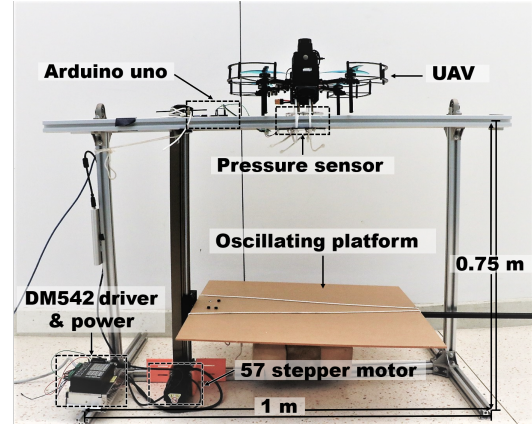


Fig. 3: GEF DC platform is equipped with a pressure sensor, an Arduino uno board and a vertical movable platform.

Experimental data (see Fig. 2) indicate that these models may not be entirely applicable to situations on mobile platforms. Furthermore, to obtain an accurate model, a large amount of real-world data to identify the unknown parameter is still mandatory. Inspired by this fact, here we endeavor to establish a purely data-driven model capable of accurately characterizing GEF encountered during UAV landing on a vertical oscillating platform. This model is employed for feedforward compensation of disturbances arising from ground effects in the drone landing process, thereby achieving a more rapid, precise, and smooth descent. Importantly, this data-driven approach does not involve any intricate neural networks, ensuring that the final model maintains the same level of simplicity as empirical models.

The aim of this paper is now formally given as follows. In consideration of the data collected during the UAV landing process, which encompasses the throttle command σ , relative height z , Z -axis velocity of UAV $v_{z,q}$ and Z -axis velocity of the platform $v_{z,p}$, our objective is to obtain a precise GEF model in the form of

$$\hat{f}_{GEF} = \mathcal{F}(\hat{f}_{GEF}, \sigma, z, v_{z,q}, v_{z,p}) \quad (3)$$

for real-time estimation of the ground effect forces induced by the aerodynamic interaction between the UAV and the vertically vibrating platform.

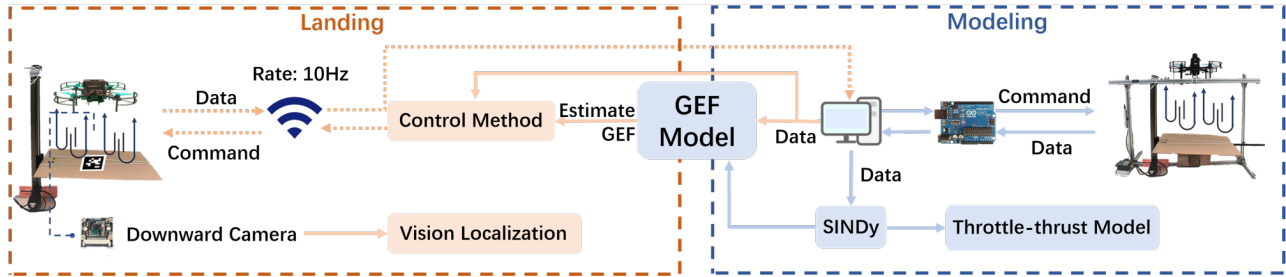


Fig. 4: The part within the blue box represents the **modeling of throttle-thrust and GEF** using SINDy and data collected from the **GEF DC platform**. The part within the orange box represents the **landing of UAV on a vertical oscillating platform**, combining the control method with the **estimated GEF** calculated by **GEF model**.

III. MODELING AND LANDING SCHEME DESIGN

In this section, we will provide a detailed procedure for the construction of the GEF model. First, a throttle-thrust model is first established. Then, we extract f_{GEF} from the overall thrust based on the throttle-thrust model. Both of these two models are derived by using the SINDy method [18]. The selections of library functions in SINDy function libraries are partially inspired by empirical formulas. By combining the GEF model with a nonlinear feedback controller [15], the UAV can achieve a fast and smooth landing on the vertical oscillating platform. Fig. 4 depicts the overall modeling and landing scheme.

A. GEF Data Collecting (DC) Platform

To acquire precise thrust data generated by the UAV, we developed a GE testing platform depicted in Fig.3, which consists of a UAV, a pressure sensor, a mobile platform and a main control board. Based on this platform, we can directly measure the real-time thrust value generated by propellers and operate the vertical oscillating platform to change f_{GEF} that occurs between the UAV and the platform. A more detailed description will be provided in Section IV-A.

B. Modeling of Throttle-Thrust and f_{GEF}

In the platform established in Section III-A, it is possible to accurately measure the thrust experienced by the unmanned aerial vehicle (UAV). When the UAV moves away from the landing platform, this force is solely generated by the propellers and follows a first-order filter in accordance with the throttle command $\sigma \in \mathbb{R}$. f_{GEF} only manifests when the UAV approaches the landing platform, but during this time, the measurements within the platform also include thrust generated solely by the propellers. Hence, it is necessary to establish a throttle-thrust model capable of accurately estimating T based on the current σ . On the basis of it, f_{GEF} can be extracted from the measured thrust data.

a) Throttle-Thrust Model: In view of a fundamental observation in [19, ch.6.1], the steady-state motor speed $\varpi_{ss} \in \mathbb{R}$ exhibits a linear relationship with σ , which has the form of $\varpi_{ss} = c_R\sigma + \varpi_b$ with $c_R = c_b U_b$. c_b and ϖ_b are constant parameters. U_b denotes the battery output voltage, which experiences relatively small variations during short duration flights.

However, there exists a response time that enforces motor speed $\varpi \in \mathbb{R}$ to reach the corresponding ϖ_{ss} , while σ is executed. The relationship can be expressed as

$$\dot{\varpi} = \frac{c_R\sigma + \varpi_b - \varpi}{T_m} \quad (4)$$

with the time constant T_m .

Thanks to $T = c_T \varpi^2$ with the rotor force coefficient c_T , we can conclude that the square root of T , referred to as $T_{sr} \in \mathbb{R}$, is directly proportional to ϖ , that is, $T_{sr} = \sqrt{c_T} \varpi$. According to Eq. (4), the dynamic of T_{sr} is obtained as:

$$\dot{T}_{sr} = \frac{\sqrt{c_T} c_R \sigma + \sqrt{c_T} \varpi_b - T_{sr}}{T_m} \quad (5)$$

Therefore, we selected the following SINDy library.

$$\Theta_T := \{1, T_{sr}, \sigma, \sigma^2, T_{sr}^3, \exp(-T_{sr})\sigma, \sin(T_{sr})\sigma\}$$

Following a procedure similar to [18], we employed sparse regression in the modeling process of SINDy to identify a small subset of active terms from the library Θ_T . In this way, the model $\mathcal{T}(\cdot)$ that relates throttle to thrust can be written in the following form:

$$\dot{T}_{sr} = \mathcal{T}(\hat{T}_{sr}, \sigma) = \Theta_T \Xi_T \quad (6)$$

where $\hat{T}_{sr} \in \mathbb{R}$ represents the estimated T_{sr} . Ξ_T is the expected sparse matrix of coefficients identified by employing Sparse Relaxed Regularized Regression (SR3) [20]. This throttle-thrust model can achieve a real-time estimation of T with the given initial thrust value and σ .

b) GEF Model: With the estimation of thrust, we can extract the real-time f_{GEF} from the measured thrust obtained from the GEF DC platform.

In Eq. (2), it can be seen that f_{GEF} is related to T and z . However, the problem we aim to solve is the landing of the UAV on the vertically oscillating platform, which is more challenging due to the variations in f_{GEF} experienced by the UAV during landing. In this scenario, the motion of the platform can be represented as a superposition of some sinusoidal functions [21]. Inspired by these, the SINDy library Θ_{GEF} is selected as follows:

$$\Theta_{GEF} := \{1, f_{GEF}, \sigma, z, v_{z,q}, v_{z,p}, \sigma^2, z^2, v_{z,q}^2, v_{z,p}^2\}$$

Following a procedure similar to (6), the GEF model admits the following form

$$\dot{f}_{GEF} = \mathcal{F}(\hat{f}_{GEF}, \sigma, z, v_{z,q}, v_{z,p}) = \Theta_{GEF} \Xi_{GEF} \quad (7)$$

where Ξ_{GEF} is expected sparse matrix of coefficients. The point to be explained here is that $v_{z,q} = a_{z,q}t + v_{0z,q}$, in

which $a_{z,q} = (f_u + f_a - mg)/m \in \mathbb{R}$ and $v_{0z,q} \in \mathbb{R}$ denotes the given initial velocity of UAV in Z -axis direction. $v_{z,p}$ is calculated by subtracting v_z from $v_{z,q}$.

C. UAV Landing Control Method Based on GEF Model

Due to our focus on UAV landings, limitations are imposed on the motion in the XY plane, UAV attitude, and aerodynamic disturbance. Therefore, the position model Eq. (1) and the residual force f_a which is considered to be generated by GE are our primary concerns. In this case, \hat{f}_{GEF} is incorporated as a feedforward term in nonlinear feedback control method [15], to achieve a fast and smooth landing.

Define the position tracking error $\tilde{\mathbf{p}} := \mathbf{p} - \mathbf{p}_d$ with the desired position $\mathbf{p}_d \in \mathbb{R}^3$, and a composite variable $\mathbf{s} \in \mathbb{R}^3$,

$$\dot{\mathbf{s}} = \dot{\tilde{\mathbf{p}}} + \Gamma \tilde{\mathbf{p}} = \dot{\mathbf{p}} - \mathbf{v}_r$$

where Γ is a positive definite matrix and $\mathbf{v}_r \in \mathbb{R}^3$ is the reference velocity. It is worth mentioning that when \mathbf{s} exponentially converges to an error ball around $\mathbf{0}$, \mathbf{p} will exponentially converge to a proportionate error ball around the desired trajectory $\mathbf{p}_d(t)$ [22]. The nonlinear feedback controller is formulated as:

$$\mathbf{f}_d = m\dot{\mathbf{v}}_r - K_P \mathbf{s} - K_I \int \mathbf{s} dt - mg - \hat{\mathbf{f}}_a \quad (8)$$

where K_P and K_I are positive definite control gain and $\mathbf{f}_d := [f_{d,x}, f_{d,y}, f_{d,z}]^\top$ represents the desired thrust output. Here $\hat{\mathbf{f}}_a := [0, 0, \hat{f}_{GEF}]^\top$, i.e. the estimated residual force only takes into account \hat{f}_{GEF} in Z -axis direction.

Substituting Eq. (8) into Eq. (1), the closed-loop dynamics is rewritten as $m\ddot{\mathbf{s}} + K_v \mathbf{s} + K_I \int \mathbf{s} dt = \epsilon$, with the estimated error $\epsilon := \mathbf{f}_a - \hat{\mathbf{f}}_a \in \mathbb{R}^3$. Consequently, $\tilde{\mathbf{p}}(t)$ will converge globally and exponentially to a bounded residual bound with respect to the norm bound of $\|\epsilon\|$ [23], [24].

IV. EXPERIMENTAL RESULTS

To comprehensively validate the feasibility of the proposed landing scheme, we conducted three sets of experiments to demonstrate its effectiveness: real-time estimation of throttle-thrust model and GEF model, as well as autonomous landing of UAV on the ground and the vertical oscillating platform. For the latter two experiments, we compared three different control methods. Through these comparisons, we were able to demonstrate the superiority and validity of our modeling and landing scheme in achieving fast and smooth landings on both the ground and the vertical oscillating platform.

A. Experiment Setup

In our experiments, we used a quadcopter UAV weighing 1.37 kg with a Jetson Xavier NX onboard Linux computer. Communication with PX4 was established via Robot Operating System (ROS) using MAVROS messages over WiFi at a frequency of 10 Hz. To address limitations with PX4Flow, such as the availability of ground feature points and suitable lighting conditions, we also employed Apriltag for localization in the XY plane.

Additionally, the specific structure of the GEF DC platform can be outlined as follows:

- (1) UAV is fixed at a height of **0.75** meters above ground.
- (2) The **pressure sensor** with a precision of **0.1g** and a weighing range of up to **10kg** is installed at the connection point between UAV and GEF DC platform to measure the real-time thrust value.
- (3) **Oscillating platform** used to simulate a UAV landing surface consists of a square acrylic plate with side length of **0.6m** and a **57** stepper motor driven by a DM542 driver. The platform is capable of operating smoothly without any impact with a load of up to **5 kg**.
- (4) **Arduino uno** serves as the control board for the platform and transmits real-time thrust data to a PC through the ROS at a frequency of **10 Hz**.

B. Data Collecting and Modeling

To obtain the throttle-thrust model, we controlled the UAV using various throttle signals, e.g. ramp signals and sinusoidal signals, and collected thrust data. Based on the collected data and employing the SINDY method, the throttle-thrust model is derived as follows:

$$\begin{aligned} \hat{T}_{sr} &= 0.215 - 0.650\hat{T}_{sr} + 13.882\sigma \\ &+ 11.815\sigma^2 - 0.123\hat{T}_{sr}^3 - 12.825\sigma^3 \\ &- 16.647 \exp(-\hat{T}_{sr})\sigma - 1.457 \sin(\hat{T}_{sr})\sigma \end{aligned} \quad (9)$$

Then, the estimated thrust \hat{T} can be calculated from $\hat{T} = \hat{T}_{sr}^2$. By subtracting the real-time measured thrust from \hat{T} , the real-time f_{GEF} at each moment can be obtained. To collect more comprehensive data, three scenarios are designed:

- (1) σ remains **constant** while the platform is **undergoing oscillating at a speed of 0.08 m/s**.
- (2) σ is set to a **sinusoidal signal** while the platform remains **stationary**.
- (3) σ is set to a **sinusoidal signal** while the platform is **undergoing oscillating at a speed of 0.08 m/s**.

Similarly, the GEF model can be obtained by employing

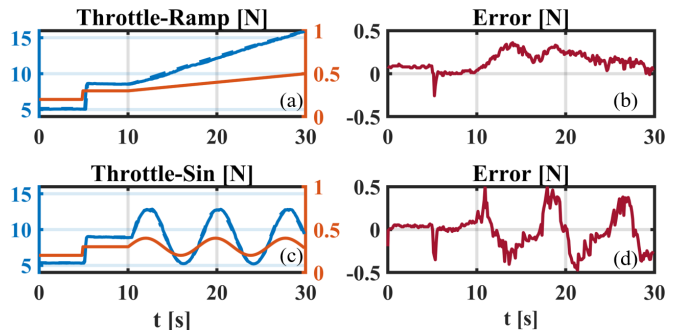


Fig. 5: Experimental results of **trottle-thrust model** estimation. (a), (b) and (c), (d) represent the results of σ is set to a ramp signal and a sinusoidal signal, respectively. In (a), (c), the **blue solid and dotted line** denote the **real-time T** and \hat{T} respectively, and **orange solid line** denotes the σ . In (b), (d), **estimated error** between **real-time T** and \hat{T} is represented by the **red solid line**. These figures demonstrate that the **trottle-thrust model** is **sufficiently accurate**.

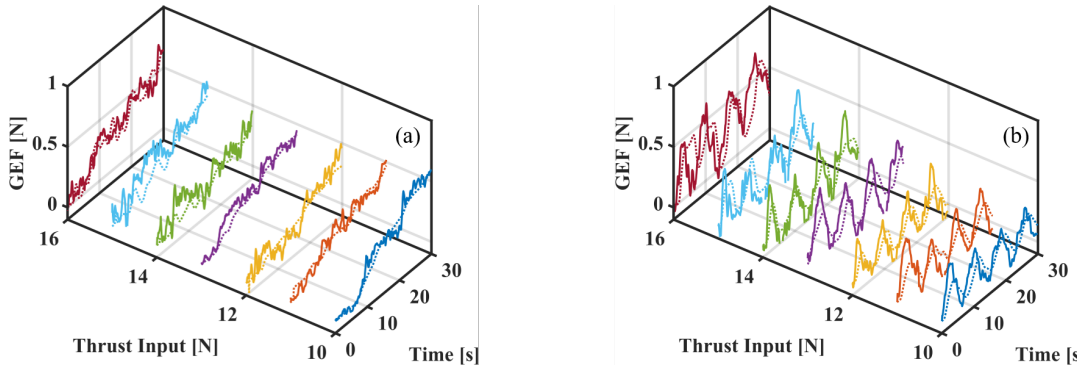


Fig. 6: Colors solid and dotted lines represent the real-time f_{GEF} and \hat{f}_{GEF} calculated by **GEF model** under different thrust input respectively. (a) indicates that our **GEF model** can accurately estimate f_{GEF} when the platform gradually **approaches** UAV. However, When the platform continues to **oscillate**, the error in (b) increases compared to (a), but it remains within an **tolerable range**.

TABLE I: GEF Model Performance Index of (a)

| Thrust [N]] | Average error [N] | Variance |
|-------------|-------------------|----------|
| 10 | 0.0436 | 0.0015 |
| 11 | 0.0469 | 0.0011 |
| 12 | 0.0657 | 0.0020 |
| 13 | 0.0529 | 0.0014 |
| 14 | 0.0840 | 0.0032 |
| 15 | 0.0989 | 0.0053 |
| 16 | 0.0732 | 0.0022 |

the SINDy method on the collected data, and it is given as:

$$\begin{aligned} \dot{\hat{f}}_{GEF} = & 0.804 - 0.088\hat{f}_{GEF} - 3.912\sigma \\ & + 0.586z + 1.051v_{z,p} - 1.049v_{z,q} \\ & + 4.854\sigma^2 + 1.103v_{z,p}v_{z,q} - 2.504z^2 \\ & - 0.535v_{z,p}^2 - 0.562v_{z,q}^2 \end{aligned} \quad (10)$$

C. Validation of SINDy Model

1) *Validation of throttle-thrust model* In the experiment, we validated the accuracy of the throttle-thrust model (9). By initially setting σ to increase from 0.2 to 0.3 and subsequently setting $\sigma = 0.1(t - 10)$, after achieving thrust stability. We observed real-time T and \hat{T} , along with the corresponding estimated error, as depicted in Fig. 5(a) and Fig. 5(b). Our throttle-thrust model demonstrated successful and accurate estimation.

Second, we set the throttle σ from 0.2 to 0.3 initially and then started to perform a sinusoidal motion $\sigma = \sin(0.8(t - 10))$. The result is displayed in Fig. 5(c) and Fig. 5(d), which demonstrate that the estimated error is still within a limitation range under a sinusoidal throttle signal.

Both results show that within a certain range of throttle variations σ , our model consistently achieves a precise thrust estimation with small deviations.

2) *Validation of GEF model* In this part, we conducted two sets of experiments where the moving platform gradually approaches UAV and oscillates at a speed of 0.08 m/s, along with an experiment duration of 30 seconds. Furthermore, both experiments consist of six individual trials. In each trial, UAV is set to generate an initial thrust of 10N, 11N, 12N, 13N, 14N, 15N, and 16N respectively,

TABLE II: GEF Model Performance Index of (b)

| Thrust [N]] | Average error [N] | Variance |
|-------------|-------------------|----------|
| 10 | 0.1051 | 0.0040 |
| 11 | 0.1292 | 0.0064 |
| 12 | 0.0947 | 0.0044 |
| 13 | 0.1507 | 0.0295 |
| 14 | 0.1080 | 0.0084 |
| 15 | 0.1127 | 0.0073 |
| 16 | 0.1958 | 0.0182 |

while remaining the throttle command unchanged. These experiments are conducted to demonstrate the effectiveness of the GEF model (10) in various scenarios.

Fig. 6 depicts the curves of real-time f_{GEF} and \hat{f}_{GEF} for both experiments. Table I and Table II show the average error and variance between f_{GEF} and \hat{f}_{GEF} with different thrust. According to Fig. 6(a) and Table I, we can conclude that as the platform gradually approaches the UAV, (10) exhibits small errors and quickly tracks the actual f_{GEF} . In Fig. 6(b) and Table II, compared to the previous experiment, the average error and variance have increased, indicating that (10) experiences some errors when there is a rapid change in the relative distance between the UAV and the platform. However, these errors still remain within a small range and have minimal impact on the landing.

D. Comparative Experiments of UAV Landing on Ground

Four sets of comparative experiments were conducted in this part, in which we compared three different control methods: no-feedforward control, feedforward control based on the empirical GEF formula, and feedforward control based on our GEF model (10). In each experiment, the UAV initiated its descent from a height of 0.8 m with a landing time constraint of 12 seconds. Taking into account the height of the landing gear, the UAV is considered to have landed when it reaches a height of 0.08 m above the ground.

In Fig. 8, the experiment results indicate the difficulty of landing a UAV on the ground without compensation. The presence of GE causes the UAV to hover around 15 cm above the ground before achieving a successful landing. Incorporating f_{GEF} , calculated using an empirical formula, into the controller improves the UAV's landing performance

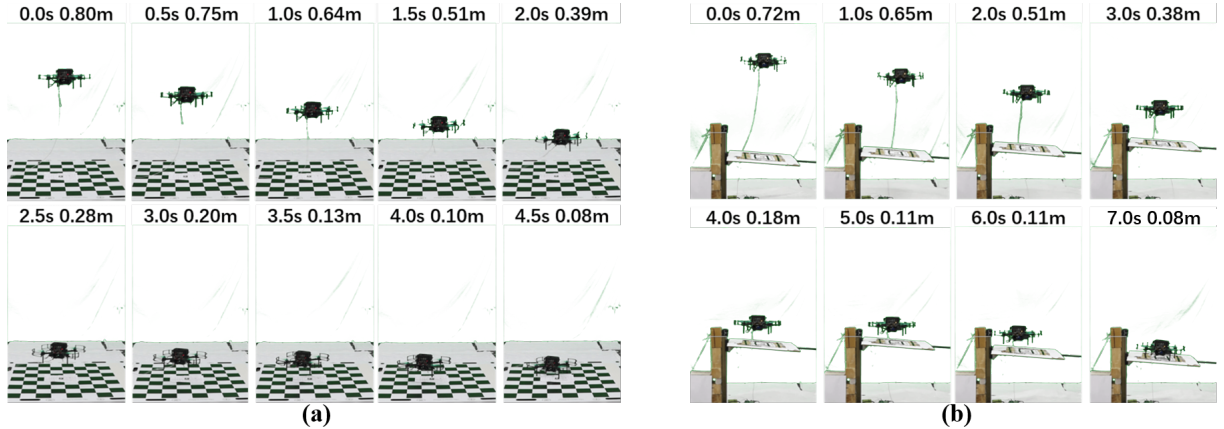


Fig. 7: (a) and (b) depict the successive stages of UAV landing on both the **ground** and **vertical oscillating platform** respectively. (a) demonstrates there is **small oscillation** that occurs during the landing process, which is also **minor** in (b). In both cases, UAV all successfully achieved **fast and smooth landing**. These illustrations validate the effectiveness of our GEF model.

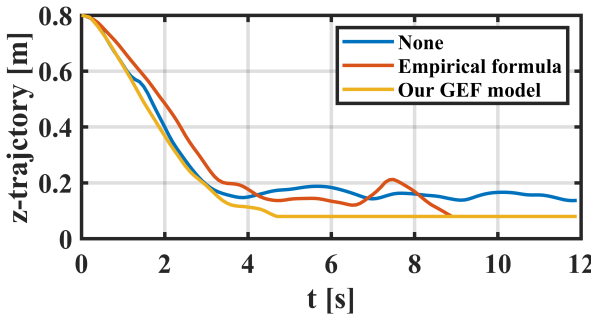


Fig. 8: This figure shows the **Z-axis trajectory** of UAV landing on the ground with three different control methods. Blue, orange and yellow lines are the results of **non-feedforward control**, **feedforward control based on the empirical formula** and **feedforward control based on our GEF model**, respectively. It is clear to see that UAV lands in a **faster and smoother manner** when the control method is combined with our GEF model.

to some extent. However, significant oscillations and a prolonged landing time still persist.

UAV landing with empirical GEF-based feedforward control have an average landing time of $\bar{t}_e = 7.1s$, while those landing with \hat{f}_{GEF} achieve an average landing time of $\bar{t}_s = 5.1s$. Without feedforward compensation, UAVs encounter considerable difficulties in achieving landings. The absence of f_{GEF} feedforward compensation presents a significant challenge to a successful landing. However, incorporating \hat{f}_{GEF} as a feedforward term leads to faster and smoother UAV landing compared to using \hat{f}_{GEF}^e .

To accurately depict the landing process, UAV positions every 0.5 seconds will be displayed in Fig. 7(a) to provide a realistic representation of the landing process.

E. UAV Landing on the Vertical Oscillating Platform

In this part, the vertically oscillating platform was set to oscillate at a speed of 0.08 m/s. By introducing \hat{f}_{GEF} as a feedforward term in the nonlinear feedback control method, the UAV successfully landed on the oscillating platform within 7 s, demonstrating the effectiveness of the proposed modeling and landing scheme. As shown in Fig. 9 and Fig. 7(b), it is clear that this scheme enables fast and smooth UAV landings on the vertically oscillating platform. Our GEF

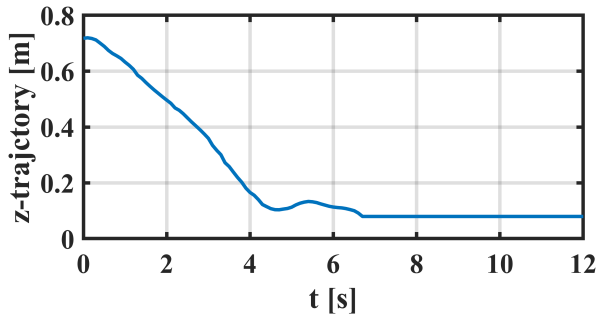


Fig. 9: Blue line depicts the **Z-axis trajectory** of UAV landing process, demonstrating the **effectiveness of our modeling and landing scheme** in achieving fast and smooth landing of UAV on the vertical oscillating platform.

model effectively addresses the challenge of UAV landing on the vertically oscillating platform, utilizing data collected from both the UAV and the platform.

V. CONCLUSIONS

In this paper, a parsimonious but accurate GEF model employing SINDy method is established, which serves as a feedforward term integrated into a nonlinear feedback control method for achieving fast and smooth landing of UAVs on the vertical oscillating platform. In addition, a GEF data collecting platform is developed to measure real-time thrust data, facilitating the modeling of both throttle-thrust and GEF, where throttle-thrust model is utilized to obtain real-time GEF from the measured thrust data collected in the GEF data collecting platform. It is noteworthy that the proposed GEF model is both sparse and interpretable, enabling effective stability analysis in combination with various control methods. Moreover, its sparsity ensures successful implementation on UAV platforms with limited computational power. Comparative experiments involving landings on the ground and the vertically oscillating platform demonstrate the feasibility of the proposed GEF model. In future work, we will explore the development of a more accurate GEF model by incorporating advanced control methods to achieve faster and smoother UAV landings. Additionally, we plan to expand our research to include UAV landings on actual moving ships.

REFERENCES

- [1] R. C. Sundin, P. Roque, and D. V. Dimarogonas, "Decentralized model predictive control for equilibrium-based collaborative uav bar transportation," in *2022 International Conference on Robotics and Automation (ICRA)*, 2022, pp. 4915–4921.
- [2] Y. Yue, C. Zhao, Y. Wang, Y. Yang, and D. Wang, "Aerial-ground robots collaborative 3d mapping in gnss-denied environments," in *2022 International Conference on Robotics and Automation (ICRA)*, 2022, pp. 10 041–10 047.
- [3] L. Heintzman, A. Hashimoto, N. Abaid, and R. K. Williams, "Anticipatory planning and dynamic lost person models for human-robot search and rescue," in *2021 IEEE International Conference on Robotics and Automation (ICRA)*, 2021, pp. 8252–8258.
- [4] B. Kiefer and A. Zell, "Fast region of interest proposals on maritime uavs," in *2023 IEEE International Conference on Robotics and Automation (ICRA)*, 2023, pp. 3317–3324.
- [5] L. Gonçalves and B. Damas, "Automatic detection of rescue targets in maritime search and rescue missions using uavs," in *2022 International Conference on Unmanned Aircraft Systems (ICUAS)*, 2022, pp. 1638–1643.
- [6] J. Jessin, C. Heinzel, N. Long, and D. Serre, "A systematic review of uavs for island coastal environment and risk monitoring: Towards a resilience assessment," *Drones*, vol. 7, no. 3, p. 206, 2023.
- [7] C. Powers, D. Mellinger, A. Kushleyev, B. Kothmann, and V. Kumar, "Influence of aerodynamics and proximity effects in quadrotor flight," in *Experimental Robotics: The 13th International Symposium on Experimental Robotics*. Springer, 2013, pp. 289–302.
- [8] Y. Zou and K. Xia, "Robust fault-tolerant control for underactuated takeoff and landing uavs," *IEEE Transactions on Aerospace and Electronic Systems*, vol. 56, no. 5, pp. 3545–3555, 2020.
- [9] F. Dong, X. Li, K. You, and S. Song, "Standoff tracking using dnn-based mpc with implementation on fpga," *IEEE Transactions on Control Systems Technology*, vol. 31, no. 5, pp. 1998–2010, 2023.
- [10] L. Xu, D. Guo, and H. Ma, "Cascade active disturbance rejection control for quadrotor uav," in *2019 Chinese Control Conference (CCC)*, 2019, pp. 8044–8048.
- [11] O. Mofid, S. Mobayen, and W.-K. Wong, "Adaptive terminal sliding mode control for attitude and position tracking control of quadrotor uavs in the existence of external disturbance," *IEEE Access*, vol. 9, pp. 3428–3440, 2021.
- [12] B.-S. Chen and T.-W. Hung, "Integrating local motion planning and robust decentralized fault-tolerant tracking control for search and rescue task of hybrid uavs and biped robots team system," *IEEE Access*, vol. 11, pp. 45 888–45 909, 2023.
- [13] B. Hu, L. Lu, and S. Mishra, "Fast, safe and precise landing of a quadrotor on an oscillating platform," in *2015 American Control Conference (ACC)*. IEEE, 2015, pp. 3836–3841.
- [14] L. Danjun, Z. Yan, S. Zongying, and L. Geng, "Autonomous landing of quadrotor based on ground effect modelling," in *2015 34th Chinese Control Conference (CCC)*, 2015, pp. 5647–5652.
- [15] G. Shi, X. Shi, M. O'Connell, R. Yu, and K. Azizzadenesheli, "Neural lander: Stable drone landing control using learned dynamics," 2018.
- [16] A. Paris, B. T. Lopez, and J. P. How, "Dynamic landing of an autonomous quadrotor on a moving platform in turbulent wind conditions," in *2020 IEEE International Conference on Robotics and Automation (ICRA)*, 2020, pp. 9577–9583.
- [17] I. Cheeseman and W. Bennett, "The effect of ground on a helicopter rotor in forward flight. 1955," *ARC R&M*, no. 3021.
- [18] U. Fasel, E. Kaiser, J. N. Kutz, B. W. Brunton, and S. L. Brunton, "Sindy with control: A tutorial," in *2021 60th IEEE Conference on Decision and Control (CDC)*, 2021, pp. 16–21.
- [19] Q. Quan, *Introduction to multicopter design and control*. Springer, 2017.
- [20] K. Champion, P. Zheng, A. Y. Aravkin, S. L. Brunton, and J. N. Kutz, "A unified sparse optimization framework to learn parsimonious physics-informed models from data," *IEEE Access*, vol. 8, pp. 169 259–169 271, 2020.
- [21] S. Zhang, "Review of vertical take-off and landing aircraft," in *2017 Second International Conference on Mechanical, Control and Computer Engineering (ICMCCE)*, 2017, pp. 53–56.
- [22] M. O'Connell, G. Shi, X. Shi, K. Azizzadenesheli, A. Anandkumar, Y. Yue, and S.-J. Chung, "Neural-fly enables rapid learning for agile flight in strong winds," *Science Robotics*, vol. 7, no. 66, p. eabm6597, 2022. [Online]. Available: <https://www.science.org/doi/abs/10.1126/scirobotics.abm6597>
- [23] X. Shi, K. Kim, S. Rahili, and S.-J. Chung, "Nonlinear control of autonomous flying cars with wings and distributed electric propulsion," in *2018 IEEE Conference on Decision and Control (CDC)*. IEEE, 2018, pp. 5326–5333.
- [24] S. Bandyopadhyay, S.-J. Chung, and F. Y. Hadaegh, "Nonlinear attitude control of spacecraft with a large captured object," *Journal of Guidance, Control, and Dynamics*, vol. 39, no. 4, pp. 754–769, 2016.